Membrane and Water Treatment, *Vol. 11*, *No. 5 (2020) 363-374*
DOI: https://doi.org/10.12989/mwt.2020.11.5.363

Water cost analysis of different membrane distillation process configurations for brackish water desalination

Jehad M Saleh[1a], Emad M. Ali[*1], Jamel A Orfi[2b] and Abdullah M Najib[2c]

[1]*Chemical Engineering Department, King Saud University, Riyadh, Saudi Arabia*
[2]*Mechanical Engineering department, King Saud University, Riyadh, Saudi Arabia*

(Received May 11, 2018, Revised November 1, 2019, Accepted December 10, 2019)

Abstract. Membrane distillation (MD) is a process used for water desalination. However, its commercialization is still hindered by its increased specific cost of production. In this work, several process configurations comprising Direct Contact and Permeate Gap distillation membrane units (PGMD/DCMD) were investigated to maximize the production rate and consequently reduce the specific water cost. The analysis was based on a cost model and an experimentally validated MD model. It was revealed that the best achievable water cost was approximately 5.1 \$/m^3 with a production rate of 8000 m^3/y. This cost can be further decreased to approximately 2 \$/m^3 only if the heating and cooling energies are free of cost. Therefore, it is necessary to decrease the MD capital investment to produce pure water at economical prices.

Keywords: water desalination; cost analysis; membrane distillation; cascade configurations

1. Introduction

Membrane distillation (MD) is an integrated thermal and membrane desalination process. The driving force for water purification is the pressure gradient maintained by temperature difference on the two sides of a hydrophobic membrane. MD has several advantages, including the decreased temperature and pressure requirements, and the increased salt rejection rates that lead to increased product quality. MD can be operated by low-grade energy sources, such as solar, geothermal, and waste heat sources. However, to-this-date commercial applications are still lacking. Its performance remains unacceptable because the process suffers from several limitations associated mainly with its very low-production rates per unit membrane area compared to reverse osmosis (Essalhi and Khayet (2015)). Moreover, because of its low-production rate its specific energy consumption is high. Therefore, enhancing the performance of the MD system is vital for its expansion and adoption as a reliable desalination process. Several experimental and theoretical investigations have been conducted to develop methods and evaluate concepts for enhancing the performance of MD systems (Alklaibi and Lior, (2004), Matsuura and Khayet, (2011), Camacho *et al*. (2013)). Recently, Thomas *et al*. (2017) systematically reviewed most of the publications in the Science Direct database from 1970 to 2016 and concluded that the MD process received increased attention and interest during the last few decades.

The permeate and brine streams often contain significant amounts of heat that should be recovered and reused to produce more fresh water. Several concepts and methods have been studied to improve the efficiency of the MD process. For example, the implementation of heat recovery systems on either the brine or permeate sides as well as the recycling of the brine have been investigated (Summers *et al*. (2012), Swaminathan *et al*. (2018)). Recently, Lokare *et al*. (2018) emphasized the significance of feed recirculation in MD systems and analyzed its influence on the overall recovery ratio and energy consumption. The success of the multistage (or multi-effect) concept in conventional, multiple effect distillation, and in multistage flash technologies, have drawn the interest and attention towards its implementation on MD systems. As an example, several other studies have focused on increasing the capacity of the module and re-claiming the supplied heat via multistage and multiple effect concepts (Lee *et al*. (2016), Lee *et al*. (2017), Khalifa *et al*. (2017), Bhausahab, (2017)), Pangarkar and Deshmukh (2015), He *et al*. (2013). Other researchers studied the use of low-cost renewable energy and waste heat sources to reduce the overall energy consumption. The integration of MD units with renewable energy sources has also been studied (Thomas *et al*. (2017), Qtaishat and Banat (2013), Banat *et al*. (2007), Lienhard *et al*. (2012), Guillen *et al*. (2011)). Appropriate integration of MD with conventional and nonconventional desalination systems is an approach that seems to have a very good impact on increasing the recovery ratio and reducing the specific energy consumption. Examples of these hybrid

*Corresponding author, Professor
E-mail: amkamal@ksu.edu.sa
[a] Ph.D.
E-mail: jsaleh@ksu.edu.sa
[b] Ph.D.
E-mail: orfij@ksu.edu.sa
[c] Student
E-mail: anmohammed@ksu.edu.sa

ISSN: 2005-8624 (Print), 2092-7037 (Online)

configurations include the MD treatment of brine using reverse osmosis (RO) or thermal units (multiple effect distillation (MED) and multistage flash (MSF)) (Matsuura and Khayet, (2011), Orfi *et al*. (2017)).

Although the MD configurations or modifications have resulted in improved water production and recovery, its economic analysis was not thoroughly investigated. For instant, MD modification may incur additional costs, thus affecting the overall cost of production. Omar *et al*., (2018) performed economic analysis of multistage vacuum membrane distillation (VMD) with and without interstate heating as well as with and without brine recirculation. They reported water cost variation with the various VMD structures and the minimum owing to a single stage VMD with brine recycling. Zheng *et al*. (2017) studied the effect of inter-stage heating on economics of multi-effect VMD. They reported an optimum water cost of 0.59$/t for four stages VMD with first stage heating. In this study, we conduct an economic analysis of various DCMD configurations available in the literature. This will help the comparison of these configurations based on the cost of water production rather than the production rate. Water cost analysis for specific MD structure is reported in the literature, here we compare the water cost for different structures to identify the best scenario. In addition, a compressive cost model is used here that include additional overlooked cost components such as cooling, pumping pretreatment and maintenances.

Table 1 Cost parameter and operating conditions

Parameter	Value
Membrane area	10 m^2
Membrane thickness	80 μm
Pore size	0.2 μm
Channel length	14 m
Channel height	0.7 m
Channel depth	0.2 mm
Porosity	0.4
Feed pressure	1.5 bar
Permeate feed pressure	1.5 bar
Intake pressure	5.9 bar
Intake pump efficiency	80%
Feed and permeate pump efficiency	60%
Electricity cost	0.08 $/kWh
Membrane cost*	50 $/$m^2$
Steam cost	3 $/1000 kg
Cooling water cost	0.1 $/1000 kg
Plant Load Factor (PLF)	0.91
Interest rate	0.08
Plant life	20 y

* Choi *et al*. (2016)

2. DCMD model and simulations

The analysis conducted in this study is based on a mathematical model for a typical DCMD unit. The detailed derivation of the model is presented in Appendix A. The model is validated using experimental data (Ali *et al*. (2018), Ali and Orfi (2018)). The characteristics of the MD membrane are listed in Table 1. Previous experimental and theoretical studies performed on a single MD by the authors indicated low-recovery ratios and high-energy demands. These conclusions are supported by other published studies (Essalhi and Khayet (2015), Winter *et al*. (2011), He *et al*., (2013)). In our simulations, the feed water was considered as brackish water with fixed properties. The feed conditions of a hot flow rate of Q_{hf} = 600 L/h and the respective hot water feed temperature and salinity of T_{hf} = 80 °C and C_{sf} = 1414 kg/m^3 were used. The specific feed temperature and salinity are representative of some wells in the Riyadh region. Cooling water is used in a counter-current manner in the permeate side at the same flow rate of the hot feed flow rate and at a temperature of T_{cf} = 25 °C. Note that some of the proposed configurations in the next section use PGMD units. We will consider the PGMD unit has the same membrane characteristics and modeling equation used for the DCMD.

3. Design structure and methodology

As mentioned earlier, the production rate of a single MD is low. Hence, different configurations have been studied to enhance the ware production of a conventional MD unit (Matsuura and Khayet, (2011), Orfi *et al*. (2017)). Usually, cascaded MD units or MD with large area are used to increase the production rate, however, this will lead to additional operational and capital costs. Therefore, it is highly beneficial to study the water production cost of these various configurations. Table 2 lists four different possible design configurations. Note some of these arrangements are inspired from the work of Kotb *et al*. (2016) where various parallel and series configurations are proposed. Option 1 represents multiple typical MD stages in series, where the brine of the first unit is heated and fed to the second unit and so on. Heating the brine is necessary because the brine exits at a low temperature, especially when an MD with a large surface area is utilized. Unlike reverse osmosis (RO), MD operates at atmospheric pressure, and the pumps are thus used for water circulation, i.e., they overcome the pressure drop of the membrane channel, which is assumed to be equal to 0.5 bar in this study. Each MD unit has its own independent condenser water circuit. The distillate of each stage is withdrawn from the condenser loop and collected in a storage tank. The condenser circuit has a pump for water circulation and a cooler to adjust the feed temperature at 25 °C. These units are excluded from the figure owing to option 1 for simplification purposes. Note that option 1 has the advantage of over utilizing the brackish water stream to maximize the recovery ratio. Option 2 presents a parallel arrangement of three single MD units. A single heater and pump are used for parallel streams. Option 2 permits the use of a larger feed flow rate to

maximize the overall throughput. Modifications of options 1 and 2 are possible as it will be discussed below. Option 3 is distinguished because it uses a single water circuit which acts as the condenser stream and a hot feed after heating. The exiting brine is cooled down to 25 °C and fed as the condenser stream to the second stage, the process is repeated recursively. Distillate is withdrawn from the condenser loop in each stage. This structure maximizes the recovery ratio and minimizes the heating demand as the permeate leaves the MD unit at a relatively high temperature, especially when the MD has a large surface area. Similarly, it minimizes the cooling demand as the brine is discharged at low temperature for long MD modules. Henceforth, we denote the condenser stream as permeate and the purified water as distillate. Option 4 is a series configuration with recycled warm permeates. The exiting permeate is added to the feed of the subsequent stage to increase the throughput. Even though the permeates is warmer than the brine, the combined stream has a low temperature that is insufficient in producing acceptable mass flux. Therefore, heating the combined feed is still necessary.

Option 5 is a parallel structure where the main feed is split into equal parallel streams each of which feeds a single MD. Each MD has its own condenser loop from which the distillate is collected and stored. Brine exiting each MD can be fully or partially recycled and added to the hot feed of the subsequent stage. The un-recycled brine is disposed. The recycled brine is expected to increase the throughput, but it will quench the feed. Therefore, an additional heater must be incorporated.

It should be noted here that configurations 3, and 4 use PGMD which is a slight variation of DCMD where the distillate is not mixed with the cold stream and withdrawn separately. This allows using salty cold water in the condenser loop. Details on the description and principle of PGMD can be found in Winter *et al*. (2011). Despite the differences between the DCMD and OGMD we will assume they have similar performance for comparison purposes.

All aforementioned configurations use three MD units for demonstration purposes, or an increased number of stages can be implemented. For clarification and visualization, the condenser water circuit and water product lines are respectively represented by dotted or dashed lines. Moreover, in all configurations, we consider equal mass rates on brine and condenser side.

4. Water cost model

The proposed process structures can maximize the water production. However, the capital investment and associated operating cost will increase accordingly owing to an increased number of processing units and the required energy demand for heating and pumping**.** Therefore, it is of interest to assess the water production cost required by these structures. The water cost model is adopted from Choi *et al*. (2016).

The capital investment consists of several elements as follows:

Table 2 Proposed configurations

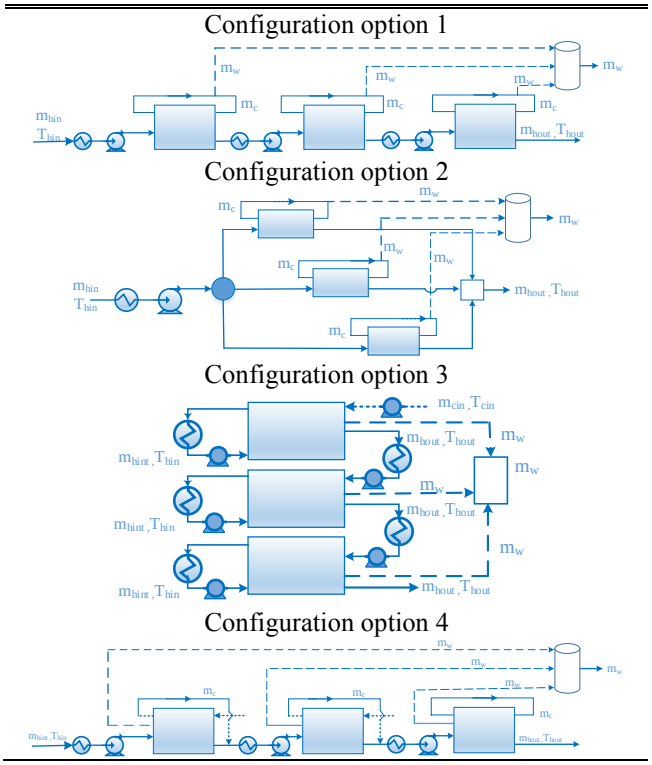

Cost of intake and pretreatment:

$$CC_{ip}(\$) = 997\left(Q_{ip}\left(\frac{m^3}{d}\right)\right)^{0.8} \quad (1)$$

Cost of feed pump:

$$CC_{FP}(\$) = 4.78 \times 10^{-6} \times Q_f(\frac{m^3}{d}) \times 120000 \quad (2)$$

Cost of heat exchanger:

$$CC_{Hx}(\$) = 1000 * Area_{HX} \quad (3)$$

where the area for heat transfer can be computed from,

$$Area_{HX} = \frac{Q_{HX}}{U_{HX}\Delta T_{lm}} \quad (4)$$

The overall heat transfer coefficient can be approximately estimated using the following correlation (El-Dessouki and Ettouney, 2002)

$$U = 1.7194 + 3.2063 \times 10^{-3}T_x + 1.5971 \times 10^{-5}T_x^2 - 1.9918 \times 10^{-7}T_x^3 \quad (5)$$

where T_x is the steam condensation temperature for heaters or the logarithmic mean temperature difference for coolers in degree Centigrade. Equation (4) is used to estimate the size of the feed heater using a saturated steam at 100 °C and the permeate cooler using a cooling water at 5 °C. A 15 °C change in the cooling utility is allowed.

The membrane cost is

$$CC_{Mem}(\$) = A_{mem}(m^2) \times C_{mem}(\frac{\$}{m^2}) \quad (6)$$

Hence, the total equipment cost is

$$CC_{eqp}(\$) = CC_{ip} + CC_{FP} + CC_{HX} + CC_{Mem} \quad (7)$$

The total and annualized capital cost can be computed as follows:

$$CC_{site}(\$) = CC_{eqp} \times 0.2 \quad (8)$$

$$DCC\ (\$) = CC_{eqp} + CC_{site} \quad (9)$$

$$ICC\ (\$) = DCC(\$) \times 0.3 \quad (10)$$

$$TCC(\$) = DCC(\$) + ICC(\$) \quad (11)$$

$$ACC\left(\frac{\$}{y}\right) = TCC(\$)\frac{i(i+1)^n}{(i+1)^n - 1} \quad (12)$$

The operating cost consists of several elements as described below. Specifically, the operating cost of intake and pretreatment is:

$$OC_{ip}\left(\frac{\$}{d}\right) = \frac{0.028P_{ip}(bar)Q_{ip}\left(\frac{m^3}{d}\right)D_{EP}(\frac{\$}{kWh})}{\eta_{ip}} \times PLF \quad (13)$$

The operating cost of feed pumping is thus expressed as

$$OC_{FP}\left(\frac{\$}{d}\right) = \frac{0.028P_{FP}(bar)Q_f\left(\frac{m^3}{d}\right)D_{EP}(\frac{kW}{h})}{\eta_{FP}} \times PLF \quad (14)$$

The cost of the steam to heat the feed is

$$OC_{steam}\left(\frac{\$}{d}\right) = Steam(\frac{kg}{d}) \times C_{steam}(\frac{\$}{kg}) \quad (15)$$

Correspondingly, the cost of cooling water, to be used for cooling the permeate whenever needed, is

$$OC_{cw}\left(\frac{\$}{d}\right) = CW(\frac{kg}{d}) \times C_{cw}(\frac{\$}{kg}) \quad (16)$$

Additionally, the total power cost is defined as

$$OC_{power}\left(\frac{\$}{y}\right) = \left(OC_{ip} + OC_{FP} + OC_{steam} + OC_{cw}\right) \times 365 \quad (17)$$

The total operating cost can be estimated as follows:

$$OC_{MR}\left(\frac{\$}{y}\right) = CC_{Mem} \times 0.2 \quad (18)$$

$$OC_{etc}\left(\frac{\$}{y}\right) = AOC \times 0.3 \quad (19)$$

$$AOC\left(\frac{\$}{y}\right) = OC_{power} + OC_{MR} + OC_{etc} \quad (20)$$

Finally, the specific cost of water production is

$$WC\left(\frac{\$}{m^3}\right) = \frac{ACC + AOC}{Q_p(\frac{m^3}{d}) \times 365 \times FLP} \quad (21)$$

The cost model will be used to estimate the water cost for the proposed configurations for comparison purposes and for determining the lowest production cost. The cost parameters of the cost model and other operating conditions are listed in Table 1. Note that the cost of cooling includes operational cost component in terms of the cost of the chilled water used for cooling and capital cost component in terms of the heat exchanger used for cooling the permeate.

5. Results and discussion

5.1 Effect of MD surface area

The MD model is validated based on the actual size of the commercial MD module which is 10 m^2. However, the model can be extrapolated to study the effect of the MD surface area on the process performance as the surface area has a direct impact on transmembrane mass and heat rates. Fig. 1 illustrates the MD performance within the range of the surface area between 1 and 30 m^2. For a small MD area of 1 m^2, $T_{h_{out}}$ is much larger than $T_{c_{out}}$ because an insufficient heat transfer area is available for heat transport across the membrane. For a large MD area of 10 m^2, $T_{c_{out}}$ becomes larger than $T_{h_{out}}$ owing to the enlarged heat transfer area. Our experimental analysis indicated that a surface area of 10 m^2 is sufficient to provide the maximum heat transfer as the brine exits at a temperature that is approximately 1 to 2 °C above the feed permeate temperature. Hence, increasing the heat transfer area beyond 10 m^2 cannot enhance the heat transfer because of thermodynamic limitations. Although the mass flux decreases for larger surface area, the overall production rate increases with the surface area as shown in Figure 1c. However, increasing the surface area beyond 10 m^2 has a marginal effect on the water cost. Both operation cost and production rate increase with stages but at different rate making their ratio to flatten as number of stages further increases. Note that the operating cost dominates the total cost and that only the cooling operating cost changes with membrane size. This makes the total cost to grow at relatively smaller rate than the production rate causing the specific total cost to level off. Ali *et al*. (2016) has also reported asymptotic value for the water cost as the membrane length increases considerably. Note, our simulations indicated that the specific water may increase slowly for stages higher than 30 if the cost of membrane per area is increased to 100 \$/m^2. Therefore, we will fix the MD surface area at this value when the proposed configurations are compared.

Fig. 1 shows the considerable effect of the feed rate on the production rate, but an insignificant impact on the water cost. In fact, the feed rate has a dual counter effect on the water's specific cost. The feed rate increases the water cost because it increases the operating cost, but at the same time it decreases the water cost because it increases the annual production. Hence, when comparing several configurations, the feed rate will be fixed at 1200 L/h to ensure enough brine circulation rate through down-stream stages. It should be noted that the best achievable water cost is approximately 25 \$/m^3 which falls within the range of 0.3 and 130 \$/m^3 reported by Essalhi and Khayet (2015).

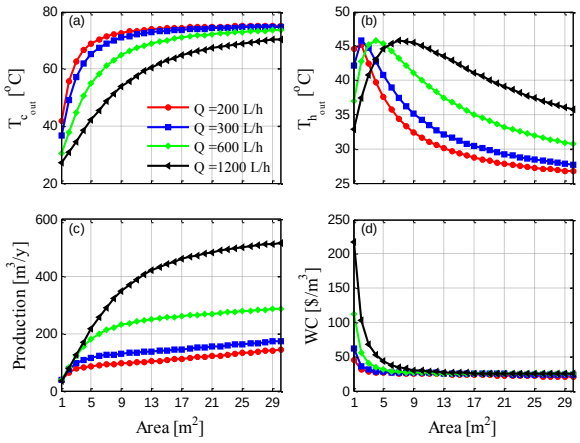

Fig. 1 Effect of MD surface area on water cost for a single MD unit

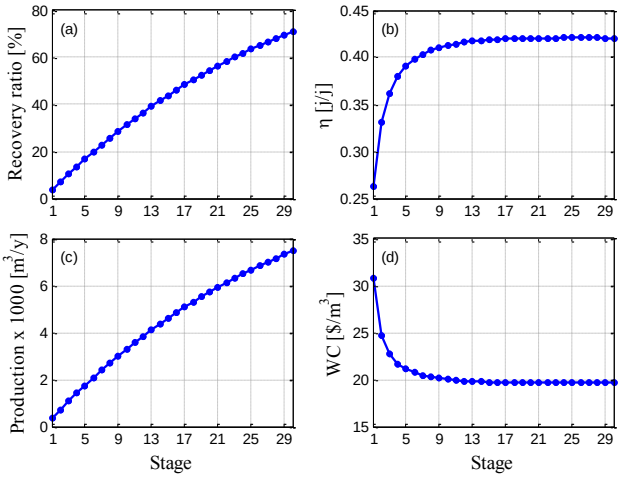

Fig. 2 Process performance for configuration 1

However, this obtained value of 25 \$/m^3 is far from what is reported by Choi *et al*. (2016) at a value of 0.95 \$/m^3. According to the authors, this water cost is based on a water production of 50000 m^3/d. Our calculations indicate that to achieve a water cost of 0.95 \$/m^3 for a water production of 50000 m^3/d requires a recovery ratio of at least 50%. This recovery ratio appears to be too high since the common recovery rate for a single MD is approximately 6.5% based on the existing experimental setup (Ali & Orfi, 2018). Summers *et al*. (2012) reported recovery ratio as low as 5%. Swaminathan *et al*. (2018) indicated the recovery ratio in a single path through MD is less than 8%. Moreover, the capacity of the MD unit used by Choi *et al*. (2016) was 14.4 m^3/d. Therefore, thousands of MD units are needed to achieve the desired production rate of 50000 m^3/d. Nevertheless, in the study by Choi *et al*. (2016) no information was provided about the number of units used and their corresponding arrangement patterns.

5.2 Comparison of the proposed configurations

Fig. 2 depicts the accumulated key process parameters for configuration option 1. The figure shows that up to 30 stages can be utilized in series until the brine flow rate is depleted, i.e., until it becomes less than the threshold of 150 L/h. This threshold is based on our experimental evaluation which indicates the minimum feed flow rate that can produce sensible water flux. It is shown that for such a unit of 30 stages, the accumulated recovery ratio and thermal efficiency can be enhanced to 78% and 41%, respectively. Moreover, the specific water cost can be reduced to approximately 20 \$/m^3 when 30 stages are used in series. Fig. 1b illustrates rapid increase in the thermal efficiency followed by saturation at 41%. Both the evaporation energy and feed heating energy grow slowly at high number of stages because both the evaporation rate and feed rate start depleting as the number of stages increases. This makes their ratio, i.e. thermal efficiency to settle at asymptotic value. Fig. 1d reveals a quick reduction in water cost at low number of stages, but as production rate builds up when more stages are added, the water cost starts leveling off. We have limited our maximum number of stages at the point where the brine flow rate reaches 150L/h. Our experimental analysis indicates a transitional process behavior when the flow rate becomes less than 150 L/h (Ali and Orfi, 2018). Below feed flow rate of 150L/h, it is observed that the mass and thermal behavior of the MD is different than that at higher flow rate. The water cost profile is in line with the literature as different variation of the water cost with number of stages is reported. Depending on the heating cost, Zhang *et al*. (2017) found that water cost may flatten as number of stages increases when electricity is used or drop sharply then start rise again with number of stages when waste energy is used. Omar *et al*. (2018) showed how the water cost decreases sharply with number of stages till it reaches a minimum. Afterward, the water cost start rising again linearly and slightly as more stages area added. Nevertheless, we have observed through simulation that the cost per capita of the membrane module, feed heating and permeate cooling influence the shape of the water cost profile. For different combination of these per unit costs, the specific water cost may start rising again especially when the number of stages exceed 30.

Fig. 3 illustrates the response of the accumulated process parameters when configuration option 2 is enforced. In this case, the principal feed flow rate is partitioned into equal parallel streams depending on the number of parallel stages. For example, we tested 6 parallel stages for two different feed flow rates, i.e. 1200 and 1800 L/h. we also test 12 parallel stages using a feed flow rate of 1200 L/h. The number of stages that can be incorporated is limited in this option by the apportioned feed flow rate for each individual stage. For example, as the number of stages increases, the apportioned parallel flow rates becomes smaller, hence a reduced production rate is obtained for each separate MD unit. Note Fig. 3 displays accumulated values. For example, the process parameter value at stage 5 is the summation of the process parameter value for all stages up to stage 5. Increasing the number of stages does not necessarily improve the process performance, as shown in the case where 12 stages are employed. Furthermore, our simulation revealed that splitting the main feed into unequal streams does not provide a significant performance enhancement. The advantage of this structure is the

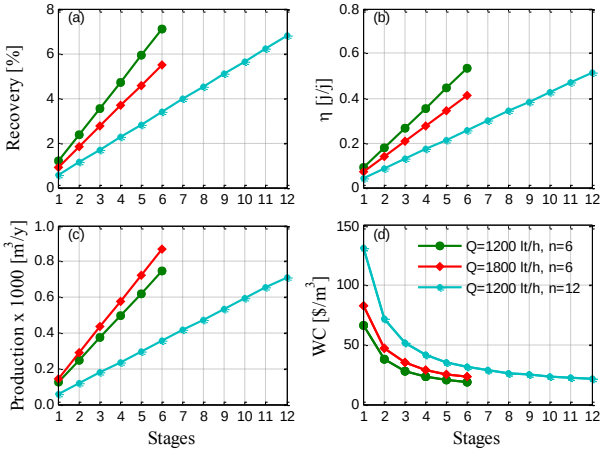

Fig. 3 Process performance for configuration 2

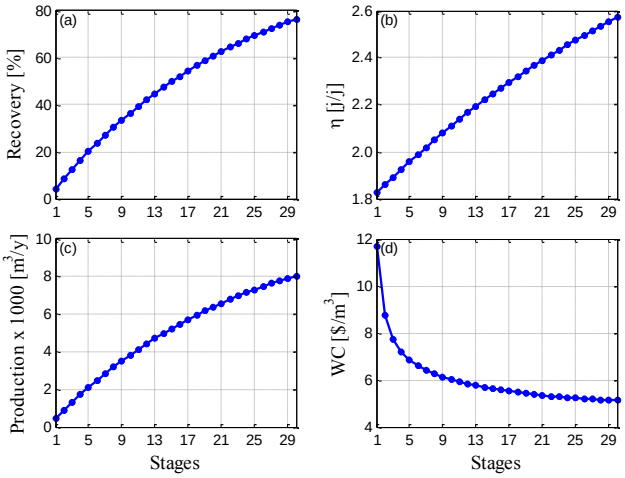

Fig. 4 Process performance for configuration 3

possibility of increasing the throughput by amplifying the feed flow rate as observed when a principal feed rate of 1800 L/h is implemented. Using 6 stages, the fed per stage is 300 L/h which results in the highest production rate (Fig. 3c). However, the high principal feed will also amplify the operating cost in terms of heating and pumping leading to a higher specific water cost. A smaller water cost is achieved when a principal feed flow rate of 1200 L/h is used and partitioned into six equal streams. A specific water cost of 21.3 $/m^2 can be obtained. Nevertheless, increasing the principal feed beyond 1200 L/h will increase the cost of water production again.

Fig. 4 demonstrates the accumulated profile of performance parameters for configuration option 3. Like option 1, many stages can be employed as long as a sufficient inter-stage feed flow is available. The latter is controlled by the water production of each individual MD unit. The performance of this option is very similar to that of option 1; however, better thermal behavior is expected. Indeed, the energy demand of the feed preheater is reduced since the recycled permeate is sufficiently warm especially if long membrane is used. Similarly, the cooling process required to quench the feed permeate is diminished because the brine temperature is usually lower than that of the warm permeate, especially when an MD with large surface area is utilized. In fact, the thermal efficiency can reach 2.6 and the water cost can be as low as 3.7 $/m^3. The maximum η and minimum WC are attained when 30 stages are used in series. Note, despite the reduction in heating and cooling demands, the operating cost still dominates the capital cost. Our simulation indicated that beyond 40 stages, the capital cost takes over and the water cost begins growing again as the overall production rate and the recovery ratio start growing asymptotically.

Fig. 5 show the accumulation of the process parameters of different stages at different recycling ratios of the warm permeate when configuration 4 is employed. In this configuration, cooling of the permeate stream is not required because it is directly mixed with the feed of the subsequent stage. By eliminating the cooling requirement, the corresponding capital and operating costs of cooling are excluded from the overall water cost. In addition, the throughput increases exponentially with the number of

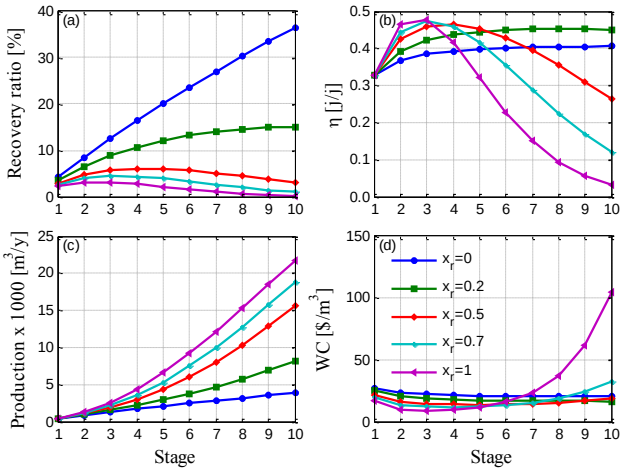

Fig. 5 Process performance for configuration option 4 at different recycle ratios, x_r

stages because it accumulates the recycled permeate stream in all preceding stages. Although the feed temperature is fixed, the feed rate for each subsequent stage increases, leading to dramatic effects on the process performance. For example, Fig. 5c shows how multifold production rate growth occurs because of the continuously increasing capacity and because of the influence of the capacity on the MD's thermal behavior. In fact, the enlarged throughput reduces the residence time which makes the permeate exit at a lower temperature and the brine at a higher temperature. This situation increases the driving force and hence the mass flux rate.

However, Fig. 5a demonstrates a decreasing recovery rate as the number of stages increases as the recovery ratio for this option is computed as the ratio of the accumulated production rate to the total accumulated feed, i.e., as the sum of the principal feed and recycled permeates. Exception is for case $x_r = 0$ because the permeate is not recycled. Similarly, η grows initially but drops as the number of stages increases especially for high recycle ratios because the energy load of the inter-stage heaters grows rapidly owing to the growing throughput. The growing energy load of the heaters amplifies the associated operating cost as well as the water cost. Note that many stages can be

Table 3 Water cost

Case	Water cost ($/m^3)	Production rate (m^3/y)
Option 1	20.0	8000
Option 2	21.3	712
Option 3	5.1	8000
Option 4	6.8	2498

used but we limit our results to 10 stages because the performance deteriorates afterward as the specific water cost grows exponentially. The minimum achievable water cost for this option is 6.8 $/m^3 when three stages are used with full permeate recycling.

A summary of the performance analysis is tabulated in Table 3. Configuration 3 leads to the minimum water cost of 5.1 $/m^3 with a high production rate of 8000 m^3/y. This value for the specific water cost is within the range reported by other authors (Camacho *et al*. (2013), Triki *et al*. (2017), Khayet (201)). For example, Camacho *et al*. (2013) reported different values for the water cost using MD values collected from different references. The specific water cost was as low as 0.26 $/m^3 and as high as 18 $/m^3. Triki *et al*. (2017) reported that a solar-driven DCMD plant with a capacity of 500 L/d can generate a water production in the range of 10–15 $/m^3. Khayet (2010) noted that the MD water cost can range from 10 to 18 $/m^3 based on the type of energy sources. He also showed that a lower water cost of 0.56 to 1.37 $/m^3 can be attained when MD is integrated with a large capacity RO plant for seawater desalination. Zhang *et al*. (2017) reported a low water cost of 0.59$/t for an optimum four stages of VMD units using waste heat with first-stage heating. Omar *et al*. (2018) reported a water cost of 1.9$/m^3 for one-stage VMD without brine recirculation. Nevertheless, the minimum water cost can still be higher than other desalination processes where the production cost can fall below 1 $/m^3. In MD, the production cost is heavily affected by the steam cost needed to heat up the feed. In addition, cooling water cost is another factor that affects the overall production cost. Although cooling water is less costly than steam, a large amount of cooling water is needed because of its smaller thermal capacity relative to steam. To show how the heating and cooling duties influence the cost, we repeat testing configuration 3 using different values of the utility cost. Fig. 6 illustrates that the minimum achievable water cost is approximately 2 $/m^3. This occurs when both the heating and cooling duty are free. The heating cost can be minimized by using waste heat, such as geothermal energy, for example. The cooling cost can be minimized when a large reservoir of cold water is available therefore permeate cooling such that recycling may not be necessary. In addition, Fig. 6 signifies the effect of cooling cost on the overall water cost. The water cost profile drops significantly when the per capita cost of cooling water reduces from 0.1 to 0.01 $/ton at a fixed steam cost of 0 $/ton. The prevalence of the cooling water cost is related to its huge flow rate compared to the steam flow rate. Note that the sensible heat of the cooling water is much smaller than the latent heat of the steam.

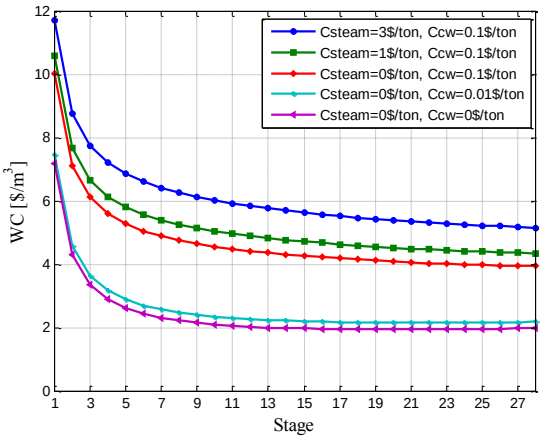

Fig. 6 Performance of option 3 for various steam and cooling water costs

6. Conclusions

MD is a promising technology for water desalination; however, its low recovery ratio and energy requirement increases the water production cost. A cost model was used to analyze the specific water cost for different process configuration scenarios. The diverse configurations were designed in a cascaded pattern such that it maximized the production rate, which in turn reduced the specific water cost. Realistic information such as those related to the membrane properties and feed and cooling temperature and flow rate values are considered in the modeling. These information data correspond to an experimental setup which was used in our previous works (Ali and Orfi (2018), Ali *et al*. (2018)). It was found that the lowest water cost was 5.1 $/m3 which can be achieved when the MD process is arranged in series with permeate heat recovery. Moreover, a single water circuit was utilized which worked as a cold permeate and hot feed simultaneously. It was also found that increasing the process throughput did not necessarily reduce the water cost because it increased the operating cost accordingly. Moreover, the cost per capita of utilities and membrane module has a significant impact on the water cost and that the cooling cots should not be overlooked. The specific water cost for this configuration can be minimized to approximately 2 $/m^3 if the heating and cooling demands are provided without cost. This minimum water cost is still higher than conventional desalination processes, such as MSF and RO. This also indicates that the initial capital investment of MD is still high and hinders the production of pure water at competetive prices.

Acknowledgement

The project was supported by King Saud University, Deanship of Scientific Research, Research Group Grant 1438–093.

References

Abdelhameed, R.M., el-deib, H.R., El-Dars, F.M.S.E., Ahmed, H. B., Emam, H.E., (2018), “Applicable Strategy for Removing

Liquid Fuel Nitrogenated Contaminants Using MIL-53-NH_2@Natural Fabric Composites", *Indsutrial Eng. Chem. Res.,* **57**(44), 15054-15065. https://doi.org/10.1021/acs.iecr.8b03936.

Ali, E. and Orfi, J. (2018), "An experimentally calibrated model for heat and mass transfer in direct contact membrane distillation", *Desalination Water Treat.*, **116**, 1-18.

Ali, E. Orfi, J. and Najib, A. (2018), "Assessing the thermal efficiency of brackish water desalination by membrane distillation using exergy analysis", *Arabian J. Sci. Eng.,* **43**, 2413-2424. https://doi.org/10.1016/j.ijheatmasstransfer.2013.07.051.

Ali, A., Quist-Jensen, C.A., Macedonio, F., Drioli, E. (2016), "Optimization of module length for continuous direct contact membrane distillation process", *Chem. Eng. Process*, **110**, 188–200. https://doi.org/10.1016/j.cep.2016.10.014.

Alklaibi, A.M. and Lior, N. (2004), "Membrane-distillation desalination: status and potential", *Desalination*, **171,** 111–131. https://doi.org/10.1016/j.desal.2004.03.024.

Banat, F., Jawied, N., Rommel, M., Koschikowski, J., and Wieghaus, M., (2007), "Desalination by a compact SMADES autonomous solar-powered membrane distillation unit", *Desalination*, **217**, 29–37. https://doi.org/10.1016/j.desal.2006.11.028.

Bhausaheb, L. P., Samir K.D., Prashant, V.T. (2017), "Multi-effect air gap membrane distillation process for pesticide wastewater treatment", *Membr. Water Treat.*, **8**(6), 539-541. https://doi.org/10.12989/mwt.2017.8.6.529.

Camacho, L. M. Dumée, L. Zhang, J. Li, J.D. Duke, M. Gomez, J. and Gray, S. (2013), "Advances in membrane distillation for water desalination and purification applications", *Water*, **5**, 94−196. https://doi.org/10.3390/w5010094.

Chen, T-C and Ho, C-D (2010), "Mediate assisted solar direct contact membrane distillation in saline water desalination", *J. Membr. Sci.* **358**, 122–130. https://doi.org/10.1016/j.memsci.2010.04.037.

Choi, Y.J. Lee, S. Koo, J. and Kim, S.H. (2016), "Evaluation of economic feasibility of reverse osmosis and membrane distillation hybrid system for desalination", *Desalination Water Treat.,* **57**, 24662–24673. https://doi.org/10.1080/19443994.2016.1152648.

Duong, H. C., Cooper, P., Nelemans, B., Tzahi Y. C., Nghiem L.D., (2015), "Optimising Thermal Efficiency of Direct Contact Membrane Distillation by Brine Recycling for Small-scale Seawater Desalination", *Desalination,* **374**, 1-9. https://doi.org/10.1016/j.desal.2015.07.009.

El-Dessouki, H. and Ettouney, H. (2002), *Fundamental of Salt Water Desalination*, Elsevier Science BV., Amsterdam, the Netherlands.

Essalhi, M., Khayet, M. (2015), "Chapter Three - Membrane Distillation (MD)", *Progress in Filtration and Separation*, Academic Press, 61-99.

Fard, K., Manawi, Y.M. Rhadfi, T. Mahmoud, K.A. Khraisheh and Benyahia, F. (2015), "Synoptic analysis of direct contact membrane distillation performance in Qatar: A case study", *Desalination*, **360**, 97–107. https://doi.org/10.1016/j.desal.2015.01.016.

Guillén, E. Blanco, J. Alarcón, D. Zaragoza, G. Palenzuela, P. and Ibarra, M. (2011), "Comparative evaluation of two membrane distillation modules", *Desalination Water Treat.*, **31**, 226–234. https://doi.org/10.5004/dwt.2011.2395.

He, F. Gilron, J. Sirkar, K. (2013), "High water recovery in direct contact membrane distillation using a series of cascades", *Desalination,* **323**, 48–54. https://doi.org/10.1016/j.desal.2012.08.006.

Khalifa, E., Alawad, S.M. and Antar, M.A. (2017), "Parallel and series multistage air gap membrane distillation", *Desalination*, **417**, 69−76. https://doi.org/10.1016/j.desal.2017.05.003.

Khayet, M. (2010), "Desalination by Membrane Distillation", *Encyclopedia of Life Support Science (EOLSS), Water and Wastewater Treatment Technologies*, EOLSS Publisher, Oxford, United Kingdom.

Kotb, H., Amer E.H., Ibrahim K.A. (2016), "On the optimization of RO (Reverse Osmosis), system arrangements and their operating conditions", *Energy*, **103**, 127-150. https://doi.org/10.1016/j.energy.2016.02.162.

Lawal, D.J. and Khalifa, A. (2014), "Flux prediction in direct contact membrane distillation", *Int. J. Material, Mechanics and Manufacture*, **2**(4), 302–308. https://doi.org/10.7763/IJMMM.2014.V2.147.

Lee, J.G., Kim, W.S. and Choi, J.S. Ghaffour, N. and Kim, Y.D. (2016), "A novel multi-stage direct contact membrane distillation module: Design, experimental and theoretical approaches", *Water Res.*, **107**, 47−56. https://doi.org/10.1016/j.watres.2016.10.059.

Lee, J-G. Alsaadi, A.S. Karam, A.M. Francis, L. Soukane, S. and Ghaffour, N. (2017), "Total water production capacity inversion phenomenon in multi-stage direct contact membrane distillation: A theoretical study", *J. Membr. Sci.*, **544**, 126–134. https://doi.org/10.1016/j.memsci.2017.09.020.

Lienhard, J.H., Antar, M.A., Smith, A., Blanco, J. and Zaragoza, G. (2012), "Solar desalination", *Annual Rev. Heat Transfer*, **15**, Article 4659.

Lokare, O.R. Tavakkoli, S. Khanna, V. and Vidic, R.D. (20180 "Importance of feed recirculation for the overall energy consumption in membrane distillation systems", *Desalination*, **428**, 250–254. https://doi.org/10.1016/j.desal.2017.11.037.

Matsuura, T. and Khayet, M. (2011), *Membrane Distillation: Principles and Applications*, Elsevier, Amsterdam, The Netherlands.

Omar, A. Nashed, A. Taylor, R. (2018), "Single Vs Multi-Stage Vacuum Membrane Distillation: An Energetic Analysis", *11th Australasian Heat and Mass Transfer Conference*, AHMTC11 9-10th July 2018, RMIT University, Melbourne, Australia.

Orfi, J. Najib, A., Ali, E., Ajbar, A., AlMatrafi, M., Boumaaza, M. and K. Alhumaizi, K. (2017), "Membrane distillation and reverse osmosis-based desalination driven by geothermal energy sources", *Desalination Water Treat.*, **76**, 40−52. http://dx.doi.org/10.5004/dwt.2017.11378.

Pangarkar B.L., and S.K. Deshmukh, S.K., (2015), "Theoretical and experimental analysis of multi-effect air gap membrane distillation process (ME-AGMD)", *J. Environ. Chem. Eng.,* **3**(3), 2127−2135. https://doi.org/10.1016/j.jece.2015.07.017.

Qtaishat, M.R. and Banat, F. (2013), "Desalination by solar powered membrane distillation systems", *Desalination*, **308**,186−197. https://doi.org/10.1016/j.desal.2012.01.021.

Safavi, M. and Mohammadi, T. (2009), "High-salinity water desalination using VMD", *Chem. Eng. J.,* **149**, 191–195. https://doi.org/10.1016/j.cej.2008.10.021.

Summers, E. Arafat, H. and Lienhard, J. (2012), "Energy efficiency comparison of single-stage membrane distillation (MD), desalination cycles in different configurations", *Desalination*, **290**, 54−66. https://doi.org/10.1016/j.desal.2012.01.004.

Swaminathan, J., Chung, H.W. Warsinger, D.M. and Lienhard J.H, (2018), "Energy efficiency of membrane distillation up to high salinity: evaluating critical system size and optimal membrane thickness", *Appl. Energy*, **211**, 715–734. https://doi.org/10.1016/j.apenergy.2017.11.043.

Thomas, N. Mavukkandy, M.O. Loutatidou, S. and Arafat, H.A. (2017), "Membrane distillation research and implementation: lessons from the past five decades", *Sep. Purif. Technol.*, **189**, 108−127. https://doi.org/10.1016/j.seppur.2017.07.069.

Triki, Z. Bouaziz M. and Boumaza, M. (2017), "Performance and cost evaluation of an autonomous solar vacuum membrane distillation desalination plant", *Desalination Water Treat.*, **73**,

107–120. http://dx.doi.org/10.5004/dwt.2017.20596.
Zhang, Y. Peng, Y. Ji, S. Qi, J. and Wang S. (2017), "Numerical modeling and economic evaluation of two multi-effect vacuum membrane distillation (ME-VMD), processes", *Desalination,* **419**, 39–48. https://doi.org/10.1016/j.desal.2017.05.032.
Zhang, J. (2011), "Theoretical and Experimental Investigation of Membrane Distillation", PhD Dissertation, Victoria University, Australia.
Winter, D., Koschikowski, J., Wieghaus, M. (2011), "Desalination using membrane distillation: Experimental studies on full scale spiral wound modules", *J. Membr. Sci.*, **375**, 1–2, 104-112. https://doi.org/10.1016/j.memsci.2011.03.030.

ED

Appendix A: DCMD desalination unit model

The mass flux (J) of the vapor transfer through the pores is given by

$$J = C_m(P_1 - P_2)\left(\frac{kg}{\frac{m^2}{s}}\right) \quad \text{(A.1)}$$

In Eq. (A.1), P_1 and P_2 are the partial pressures of water vapor estimated at the membrane surface temperatures T_{mf} and T_{mp}, respectively. The partial pressure in Pa is estimated using Antoine's equation (Lawal and Khalifa, (2014), Fard *et al*. (2015)),

$$P_1 = \exp\left(23.238 - \frac{3841}{T_{hm} - 45}\right)(1 - C_s)(1 - 0.5C_s - 10C_s^2) \quad \text{(A.2)}$$

$$P_2 = \exp\left(23.238 - \frac{3841}{T_{cm} - 45}\right) \quad \text{(A.3)}$$

where C_s is the water salinity in percent, and C_m is the MD coefficient calculated from three correlations depending on the type of the mass transfer regime.
Knudson flow mechanism:

$$C_m^k = \frac{2\varepsilon r}{3\tau\delta}\left(\frac{8M_w}{\pi RT}\right)^{1/2} \quad \text{(A.4)}$$

Molecular diffusion mechanism:

$$C_m^D = \frac{\varepsilon}{\tau\delta}\frac{PD}{P_a}\frac{M_w}{RT} \quad \text{(A.5)}$$

Knudsen molecular diffusion transition mechanism:

$$C_m^C = \left[\frac{3}{2}\frac{\tau\delta}{\varepsilon r}\left(\frac{\pi RT}{8M_w}\right)^{1/2} + \frac{\tau\delta}{\varepsilon}\frac{P_a}{PD}\frac{RT}{M_w}\right]^{-1} \quad \text{(A.6)}$$

These different regimes depend on the wall collision theory of water molecules and each regime dominates at a specific range of values regarding the mean free path of the water molecule. The heat transfer process occurs in three steps:

i. Convection from the feed bulk to the vapor–liquid interface at the membrane surface:

$$q_f = h_f(T_h - T_{mh}) \quad \text{(A.7)}$$

ii. Convection from the vapor–liquid interface at the membrane surface to the permeate side:

$$q_p = h_p(T_{mc} - T_c) \quad \text{(A.8)}$$

where h_f and h_p denote the heat transfer coefficients on the feed and cold stream sides, respectively.

iii. Evaporation and conduction through the microporous membrane:

$$q_m = JH_v + h_m(T_{mh} - T_{mc}) \quad \text{(A.9)}$$

where H_v is the water's latent heat which can be estimated using Eq. (A.10) (Fard *et al*. (2015)), whereas h_m is the conductive heat transfer coefficient and is equal to

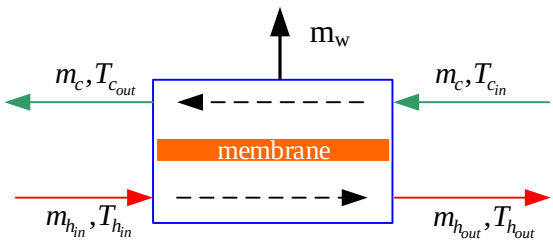

Fig. A.1: Typical DCMD unit

k_m/δ, where k_m and δ denote the membrane thermal conductivity and its thickness, respectively.

$$H_v(T) = 1850.7 + 2.8273T - 1.6 \times 10^{-3}T^2 \quad \text{(A.10)}$$

The total heat flux across the membrane is directly proportional to the bulk temperature gradient and can be expressed as follows:

$$Q = U(T_h - T_c) \quad \text{(A.11)}$$

For countercurrent flow, the bulk temperatures are taken as $T_h = T_{h_{in}}, T_c = T_{c_{out}}$.
The overall heat transfer coefficient is given by

$$U = \left[\frac{1}{h_f} + \frac{1}{h_m + \frac{JH_v}{T_{mh} - T_{mc}}} + \frac{1}{h_p}\right]^{-1} \quad \text{(A.12)}$$

Under steady state operation, the heat transfer in the three individual parts of the system reaches equilibrium:

$$q_f = q_m = q_p \quad \text{(A.13)}$$

Considering the macroscopic scale of the MD unit (Fig. A.1), the heat balance around the permeate side is given by Zhang (2011):

$$UA_s(T_h - T_c) = m_c\rho\mathrm{Cp}\left(\mathrm{T_{cout}} - \mathrm{T_{cin}}\right) \quad \text{(A.14)}$$

where m_c and C_p denote the volume flow rate and specific heat at a constant pressure, respectively. Eq. (A.14) is used to compute the permeate's exit temperature, $T_{c_{out}}$. Similarly, assuming a constant density and heat capacity, the mass and heat balance around the feed side is given by

$$UA_s(T_h - T_c) = m_{h_{in}}\rho\mathrm{Cp}\left(\mathrm{T_{h_{out}}} - \mathrm{T_{ref}}\right) - m_{h_{out}}\rho\mathrm{Cp}\left(\mathrm{T_{h_{in}}} - \mathrm{T_{ref}}\right) \quad \text{(A.15)}$$

$$m_{h_{in}} - m_{h_{out}} = m_w \quad \text{(A.16)}$$

$$m_w = JA \quad \text{(A.16a)}$$

Eq. (A.15) is used for computing $T_{h_{out}}$. It should be noted that Eqs. (A.14) and (A.15) are based on the ideal case where heat losses are negligible. Additional terms can be added to account for heat losses as a percentage of the total heat transfer to make the calculated $T_{c_{out}}$ *and* $T_{h_{out}}$ values match the experimental values. Throughout the manuscript, $m_{h_{in}}$ is also defined as the hot feed flow m_{hf}, $m_{h_{out}}$ as the brine flow m_r, $T_{h_{in}}$ as the hot feed

temperature T_{hf}, and $T_{h_{out}}$ as the brine temperature T_b. The definitions of the various variables, the numerical values of physical and design parameters in Eqs. (A.1–A.16), and additional supporting correlations are provided in (Chen and Ho, (2010), Safavi and Mohammadi (2009)).

The KPI for the MD process, such as the recovery rate and thermal efficiency, can also be defined as follows:

$$Rc = m_w/m_{h_{in}} \tag{A.17}$$

$$\eta = \frac{H_v}{H_{in}} = \frac{JA\lambda}{m_{h_{in}} Cp(T_{h_{in}} - T_{ref})} \tag{A.18}$$

When permeate heat recovery is utilized, the thermal efficiency is modified as follows,

$$\eta = \frac{H_v}{H_{in}} = \frac{JA\lambda}{m_{h_{in}} Cp(T_{h_{in}} - T_{c_{out}})} \tag{A.19}$$

Nomenclature

6	MD surface area, m^2
A	MD cross sectional area, m^2
A_{mem}	Membrane surface area, m^2
$Area_{HX}$	Heat exchanger surface area, m^2
ACC	Annual capital cost, \$/y
AOC	Annual operating cost, \$/y
C_m	Permeability coefficient, $kg/m^2.s.Pa$
C_m^k	Knudsen mass flux coefficient, $kg/m^2.s.Pa$
C_m^d	Molecular diffusion mass flux coefficient, $kg/m^2.s.Pa$
C_m^c	Transition mass flux coefficient, $kg/m^2.s.Pa$
C_s	Salinity of brackish water, kg/m^3
C_p	Heat capacity, J/kg.K
C_{mem}	Cost of membrane per area, $\$/m^2$
C_{steam}	Steam cost per kg, \$/kg
CC_{ip}	Intake & pretreatment capital cost, \$
CC_{FP}	Feed pump capital cost, \$
CC_{HX}	Heat exchanger capital cost, \$
CC_{Mem}	Membrane capital cost, \$
CC_{eqp}	Total equipment capital cost, \$
CC_{site}	Site location capital cost, \$
DCC	Direct capital cost, \$
D_{EP}	Electricity bill, \$/kWh
d_h	RO channel Hydraulic diametert, m
H_v	Heat of vaporization, J/h
H_{in}	Enthalpy of hot feed in MD unit, W
h_f, h_p, h_m	Feed, permeate, and membrane heat transfer coefficient, $W/m^2.K$
i	Interest rate, %
ICC	Indirect capital cost, \$
J	Mass flux in MD module, $kg/m^2.h$
k_m	MD membrane conductivity, W/m.K
M_w	Molecular weight of water, gm/mole
$m_{h_{in}}, m_{hout}$	Hot water inlet and outlet flow rate, kg/h
m_c	Cold water volumetric flow rate, kg/h
m_w	Permeate and distillate flow rate, kg/h
n	Plant life, y
OC_{ip}	Intake operating cost, \$/d
OC_{FP}	Feed pump operating cost, \$/d
OC_{steam}	Steam operating cost, \$/d
OC_{cw}	Cooling water operating cost, \$/d
OC_{MR}	Membrane replacement operating cost, \$/d
OC_{etc}	Other operating costs, \$/d
OC_{power}	Total power operating cost, \$/d
p_{ip}	Intake pump pressure, bar
p_{FP}	Feed pump pressure, bar
P_f, P_b	Feed and brine pressure, bar

P_1, P_2	Vapor pressure at feed and permeate membrane surface, Pa
PD	Membrane pressure multiplied by diffusivity, Pa.m^2/s
P_a	Entrapped air pressure, Pa
PLF	Plant load factor
q_f, q_p	Heat transfer rate at feed and permeate sections, W/m^2
q_m	Heat of evaporation and conduction, W/m^2
Q	Overall heat flux, W/m^2
Q_f	Feed flow rate, m^3/d
Q_{HX}	Energy load of heat exchanger, W
Q_{ip}	Intake flow rate, m^3/d
Q_p	Production rate, m^3/d
Rc	Recovery ratio, %
Re	Reynolds number
r	MD pore size, m
R	Ideal gas constant, J/mole.K
Sc	Schmidt number
Sh	Sherwood number
T, T_0	Feed water and reference temperatures, °C
T_h, T_c	Feed (hot) and permeate (cold) bulk temperatures, K
T_{mh}, T_{mc}	Feed and permeate membrane temperatures, K
T_{ref}	Reference temperature, K
T_x	Temperature for the heat transfer correlation, K
TCC	Total capital cost, $
u	Water velocity in feed channel, m/h
U	Overall heat transfer coefficient, W/m^2.K
U_{HX}	Overall heat transfer coefficient, kW/m^2.K
WC	Water cost, $/m^3

Greek

λ	Latent heat of vaporization, J/kg
η_{ip}	Intake pump efficiency
η_{FP}	Feed pump efficiency
η	Thermal efficiency
ε	Termination criteria for algorithms
ε_m	MD porosity
ν	Kinematic viscosity, m^2/h
τ	MD membrane tortuosity
δ	MD membrane thickness, mm
ρ	Density, kg/m^3